TSRR

IFAC-TSRR vol. 8 (2016) 67-78

# Diffusion-Weighted MR imaging: Clinical applications of kurtosis analysis to prostate cancer

Andrea Barucci[1,*], Roberto Carpi[2], Marco Esposito[2], Maristella Olmastroni[2], Giovanna Zatelli[2]

([1]) Istituto di Fisica Applicata "Nello Carrara" del CNR (IFAC-CNR)
([2]) Azienda USL Toscana Centro, Piazza Santa Maria Nuova 1, Firenze, Italy

([*]) A.Barucci@ifac.cnr.it


ISSN 2035-5831

## 1 - Introduction

Magnetic resonance imaging technique known as DWI (diffusion-weighted imaging) allows measurement of water diffusivity on a pixel basis for evaluating pathology throughout the body and is now routinely incorporated into many body MRI protocols, mainly in oncology [1-5]. Indeed water molecules motion reflects the interactions with other molecules, membranes, cells, and in general the interactions with the environment. Microstructural changes as e.g. cellular organization and/or integrity then affect the motion of water molecules, and consequently alter the water diffusion properties measured by DWI. Then DWI technique can be used to extract information about tissue organization at the cellular level indirectly from water motion.

In general the signal intensity in DWI can be quantified by using a parameter known as ADC (Apparent Diffusion Coefficient) emphasizing that it is not the real diffusion coefficient, which is a measure of the average water molecular motion. In the simplest models, the distribution of a water molecule diffusing in a certain period of time is considered to have a Gaussian form with its width proportional to the ADC [6,7]. However, water in biological structures often displays non-Gaussian diffusion behavior, consequently the DWI signal shows a more complex behavior that need to be modeled following different approaches.

In this work we explore the possibility to quantify the degree to which water diffusion in biologic tissues is non-Gaussian introducing the AKC parameter (Apparent Kurtosis Coefficient). DKI was first described by studies in 2004 [8] and 2005 [9] and initially was applied exclusively for brain imaging [10-12], while in recent years some studies have shown the feasibility of applying DKI at multiple extra-cranial sites [13-18].

In this work we have realized DWI non-Gaussian diffusion maps to be used in the clinical routine along with standard ADC maps, giving to the radiologist another tool to explore how much structure inside a voxel is organized.

In particular in this work some prostate DWI examples have been analyzed and will be shown. References to other studies using DKI in detection and characterization of prostate cancer can be found here [1,14,19–38,49,61-63].

## 2 - An introduction to Water Diffusion

A complete description of the diffusion theory and DWI technique is beyond the scope of this article, so here we introduce some important concepts and equations, leaving some references [2-4] for the interested readers.

Diffusion measurements in MRI usually can be performed using the standard diffusion-weighted pulse sequence (spin-echo echo-planar imaging) [39-41], obtaining images called DWI. DWI is performed by serially imaging the same tissue while varying the degree of water diffusion sensitization. The imaging gradient strength, direction, and temporal profile affect sensitivity to diffusion and are commonly reduced to a single simplified parameter referred to as the b-value [unit: s/mm$^2$]. The images obtained at different b-values are subsequently used for computing a parametric map that allows quantitative assessment of the tissue's water diffusion behavior.

In this context the corresponding echo attenuation in a voxel can be expressed as

$$S(b) = S_0 \times \exp(-b \times ADC)\,, \tag{1}$$

where *S* is the signal intensity (a.u.), depending upon the apparent diffusion coefficient (ADC) and the diffusion-sensitizing factor, which can be calculated for a spin echo sequence with rectangular diffusion-encoding gradients as follows [40]:

$$b = \gamma^2 G^2 \delta^2 \left(\Delta - \frac{\delta}{3}\right). \quad (2)$$

Here, $\delta$ is the duration of one diffusion-encoding gradient lobe, $\Delta$ is the time interval between the leading edges of the gradient lobes, $G$ is the strength of the gradient, and $\gamma$ the gyromagnetic ratio.

Then a fit on a voxel basis of equation (1) as a function of different b-values gives the ADC map that can superimposed on the standard anatomical images in order to obtain more information on the tissue under investigation.

However, biological tissues are highly heterogeneous media that consist of various compartments and barriers with different diffusivities. In terms of its cytohistologic architecture, a tissue can be regarded as a porous structure made up of a set of more or less connected compartments in a networklike arrangement.

The movement of water molecules during diffusion-driven random displacement is then impeded by compartmental boundaries and other molecular obstacles in such a way that the actual diffusion distance is reduced, compared with that expected in unrestricted diffusion. This is the reason for which the classical model of diffusion used in MRI is not always correct and must be thought as an approximation in many situations. Instead water in biological structures shows often non-Gaussian diffusion behavior. As a result, the MR signal intensity decay in tissue is not a simple mono-exponential function of the b-value [1,15,42] as described in equation (1).

Several approaches have been used to model the nonlinear decay of DWI signal intensity when more than 2 b-values are acquired. These approaches include bi-exponential fitting, from which 2 components that hypothetically reflect 2 separate biophysical compartments can be derived [43], stretched-exponential fitting, which describes diffusion-related signal intensity decay as a continuous distribution of sources decaying at different rates [44], and diffusional kurtosis analysis, which takes into account non-Gaussian properties of water diffusion by measuring the kurtosis [9].

Kurtosis represents the extent to which the diffusion pattern of the water molecules deviates from a perfect Gaussian curve. Unlike the bi-exponential model, the stretched-exponential and the kurtosis methods do not make assumptions regarding the number of biophysical compartments or even the existence of multiple compartments [45]. From the kurtosis analysis the apparent diffusion coefficient (ADC) and the apparent kurtosis coefficient (AKC) can be estimated, which are phenomenological parameters [1] supported by observations and with no direct biophysical correlation.

What we can observe is that more organized is a structure of parenchyma, much more constrains a water molecules can explore during diffusion process [1,42,46-48]. Furthermore any modification of cellular arrangements, cell size distributions, cellular density, extracellular space viscosity, glandular structures, and integrity of membranes or to measure any modification of macromolecule's concentration, translates in some features of ADC and AKC. However an interpretation of ADC and AKC is still now no straightforward [9,50-58].

The AKC parameter (adimensional) can be inserted in the mathematical signal formulation as follows:

$$S(b) = S_0 \times \exp\left(-b \times ADC + {}^1\!/_6\, AKC \times b^2 \times ADC^2\right). \quad (3)$$

This quadratic model shows a better agreement in many tissues as shown in the example of Fig. 1.

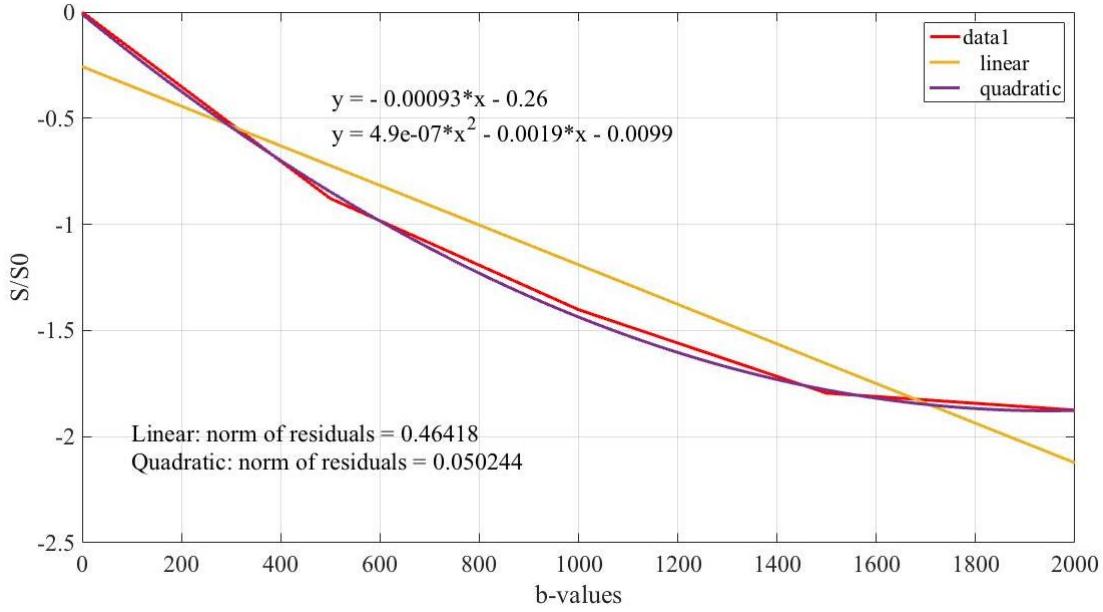


**Fig. 1** - Examples of data fitting with linear and quadratic models. The quadratic model incorporating the Kurtosis term shows a better norm of residuals in respect to the linear model. Data coming from a patient affected by prostate cancer.

AKC equals 0 when water is experiencing completely Gaussian diffusion [1], while biologic tissues tend to exhibit AKC values between 0 and 1. Studies also suggest lowering of K in the setting of post-treatment tumor necrosis [59,60]. Post-processing software commonly applies a maximal possible upper limit for AKC, above which the value is likely to represent an outlier due to motion, noise, or other artifact [1,9,55].

## 3 - Materials and Methods

Using the Philips Achieva 1.5 T available for clinical routine use at the Santa Maria Nuova Hospital in Florence we acquired a dataset of 20 patients affected by suspected prostate cancer calculating for each the ADC and AKC maps. A set of 5 b-values (0, 500, 1000, 1500, 2000 s/mm$^2$) was chosen as a trade-off for clinical use and best signal-to-noise ratio in DWI [1]. Usually b-values above 1000 s/mm$^2$ are necessary to successful capture the non-gaussian behavior.

Special software has been developed in the MATLAB framework in order to open and elaborate the DICOM images coming from the MR scanner. This software allows the data elaboration of DWI images realizing ADC and AKC maps (Figs. 2-6), at the same time introducing some post-processing tools (as moving average filter or interpolating algorithm) in order to support radiologists in the images interpretation.

## 4 - Results

DWI images have been acquired for all the patients' dataset, estimating ADC and AKC on voxel basis using Eq. (2).

Radiologists on clinical practice, cross-correlating these results with the other coming from standard MRI examination and patient clinical report, have used the obtained ADC and AKC maps.

An example of ADC and AKC maps is shown in Fig. 1.

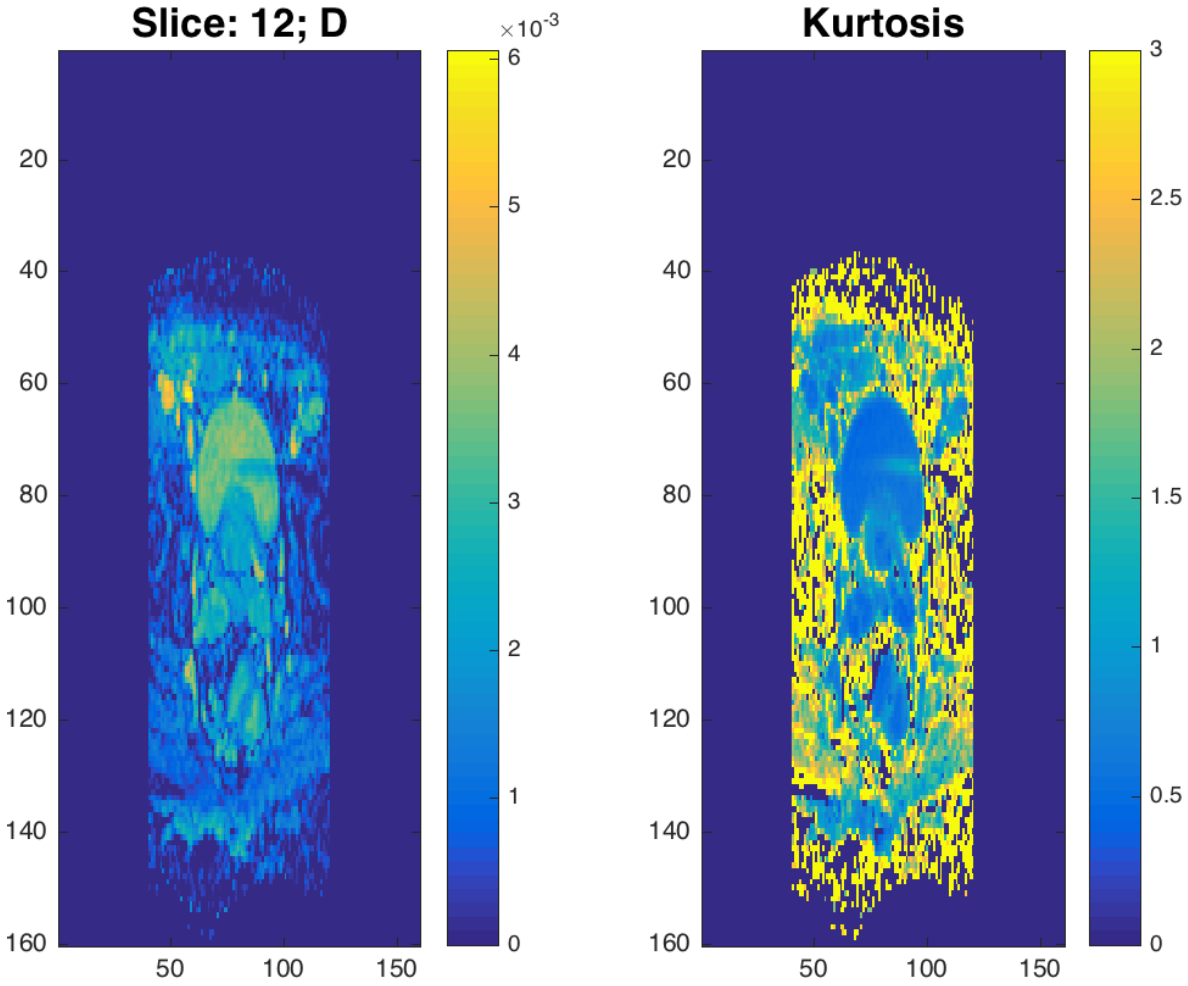


**Fig. 2 -** Example of ADC ("D") and AKC ("Kurtosis") for a patient slice.
In this case the color is different from the standard gray scalar of radiology.

Figure 3 is an example of ADC and AKC maps before and after post-processing with data interpolation. The color scale in this case is the standard for radiologists. This is just an example of the software developed for DWI data analysis.

In Fig. 4 and Fig. 5 two examples of ADC tridimensional view are shown for two patients, while for Patient 2 the AKC tridimensional view is shown in Fig. 6.

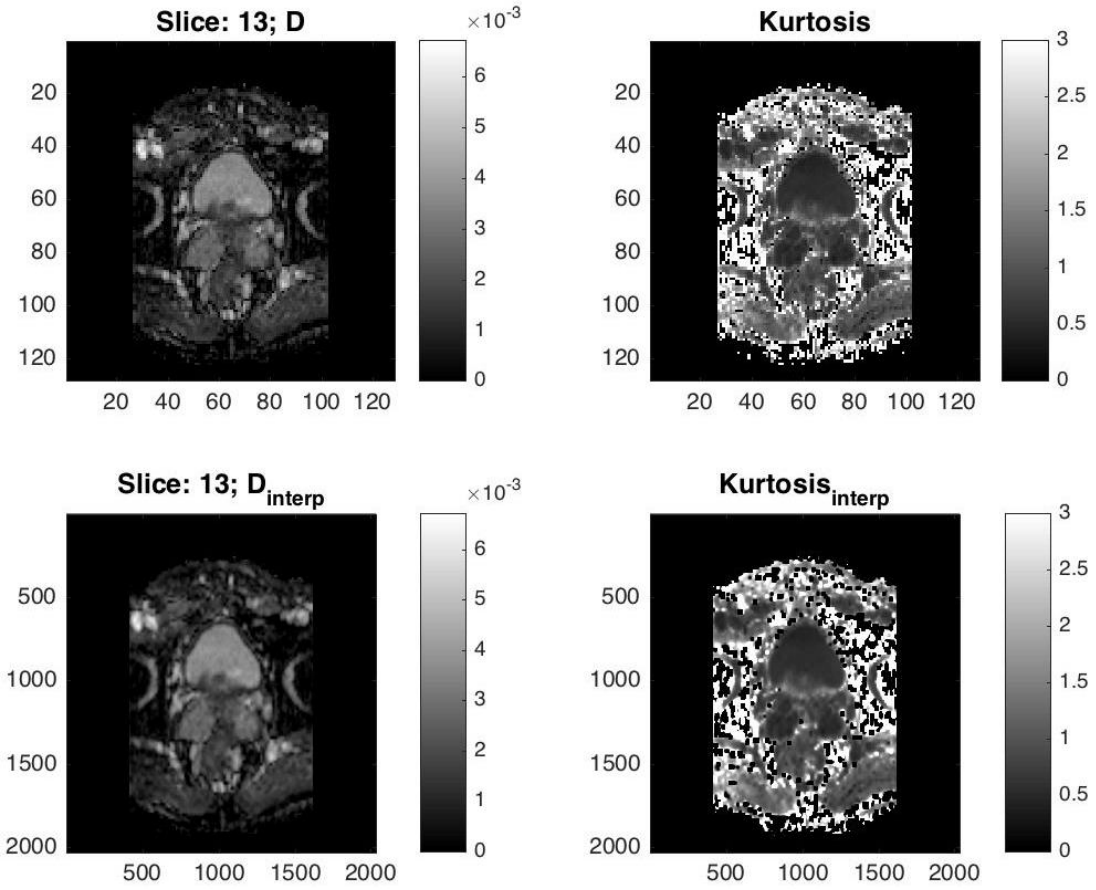


**Fig. 3 -** Examples of ADC ("D") and AKC ("Kutosis") parameters for a patient slice. In the first line the original coefficients, while in the second line the maps were interpolated in order to obtain a better resolution.

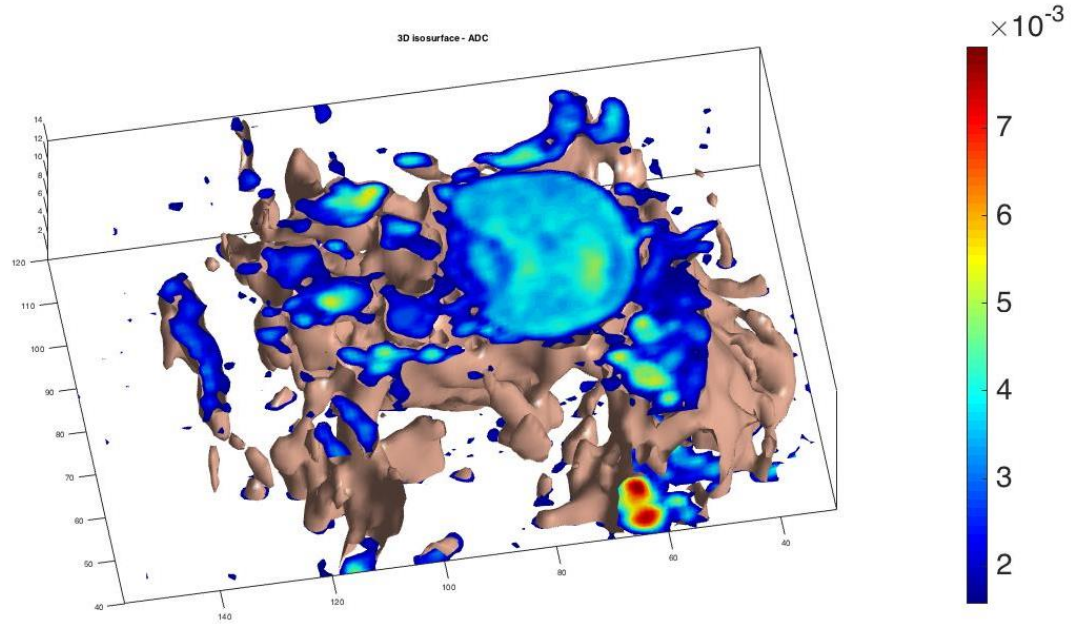


**Fig. 4 -** Example of a tridimensional ADC map for patient 1.

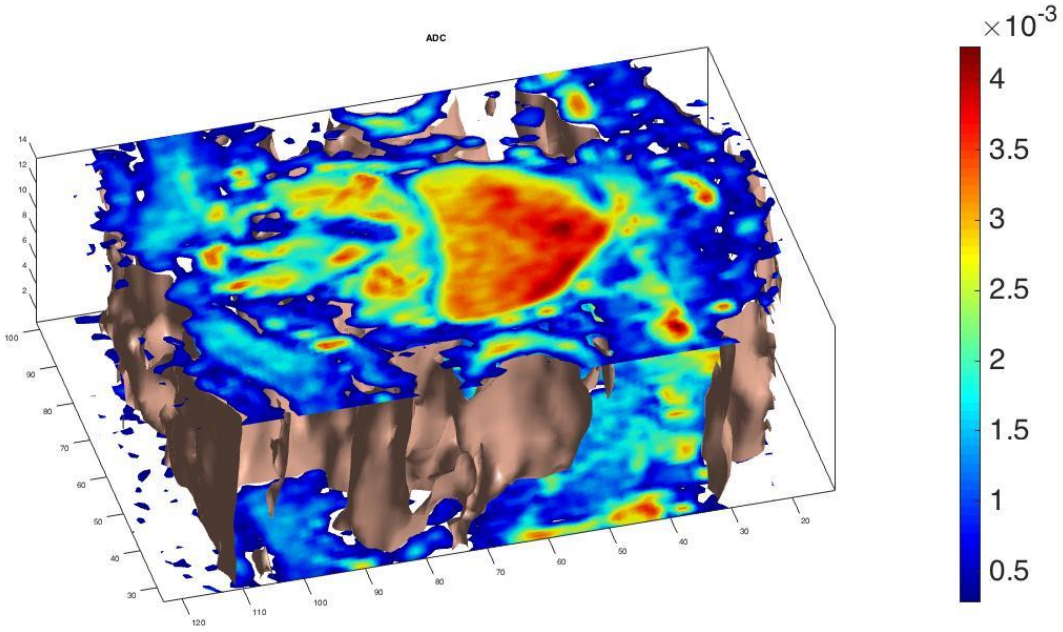


**Fig. 5 -** Example of ADC for patient 2 in a tridimensional view.

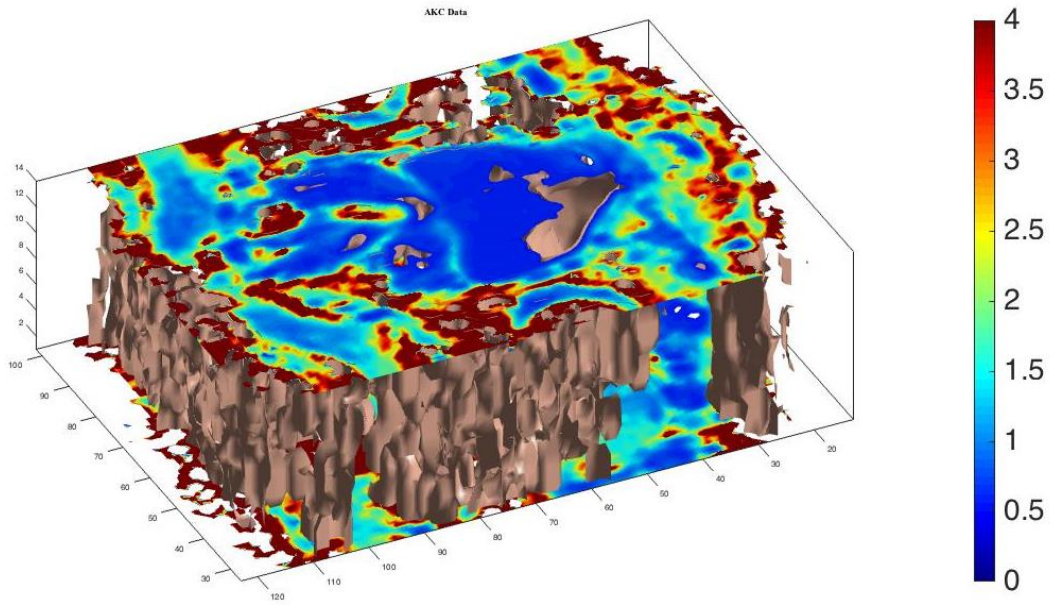


**Fig. 6 -** Example of AKC tridimensional view for patient 2.

## 5 - Conclusions

DWI non-Gaussian analysis has shown the potential to become a powerful tool in supporting radiologists in the clinical practice.

However much work remains to be done to fully understand the mechanisms underlying non-Gaussian diffusion, and the precise bio-structural significance of AKC in relation to microstructural properties of tissues.

In this framework we are working on a new and different approach based on the theoretical physics of diffusion in complex medium [64-67]

At the same time we are working on some kind of nanoparticles as a new theranostic agent for MRI applications, in particular trying to understand if nanoparticles can be revealed by diffusion-MRI techniques, looking at the change in water motion due to the presence of nanoparticles in the environment [68,69].

## 6 - Acknowledgments

The authors wish to thank Fulvio Ratto, Sonia Centi, Francesco Baldini, Ambra Giannetti and Roberto Pini, from IFAC-CNR for supporting and fruitful discussions, and the project IRINA - "Imaging Molecolare di risonanza magnetica della biodistribuzione di nanoparticelle e vettori cellulari per applicazioni teranostiche" by "Ente Cassa di Risparmio di Firenze" for financial support [Rif. Pratica n. 2015.0926, Sede Legale: via Bufalini 6, 50122 Firenze, www.entecarifirenze.it].

## References

[1]. Rosenkrantz, A. B., Padhani, A. R., Chenevert, T. L., Koh, D.-M., De Keyzer, F., Taouli, B. and Le Bihan, D. (2015), Body diffusion kurtosis imaging: Basic principles, applications, and considerations for clinical practice. J. Magn. Reson. Imaging, 42: 1190–1202. doi:10.1002/jmri.24985

[2]. Mori, S., Barker, P.B., Diffusion Magnetic Resonance Imaging: Its Principle and Applications, The Anatomical Record (New Anat.), Volume 257, Issue 3, pages 102–109, 15 June 1999

[3]. Bammer, R., Basic principles of diffusion-weighted imaging, European Journal of Radiology, Volume 45, Issue 3, March 2003, Pages 169–184

[4]. Hagmann, P., Jonasson, L., Maeder, P., Thiran, J.-P., Van J. Wedeen, and Meuli, R., Understanding Diffusion MR Imaging Techniques: From Scalar Diffusion-weighted Imaging to Diffusion Tensor Imaging and Beyond, RadioGraphics 2006 26:suppl_1, S205-S223

[5]. Giannelli, M., Lazzeri, M., Tecniche MRI per lo studio di processi di diffusione cerebrale, AIFM - Associazione Italiana di Fisica in Medicina, III Congresso Nazionale, Mediterranean Medical, Physics Meeting, Agrigento Palazzo dei Congressi 24 -28 Giugno 2003

[6]. Basser. P.J. , Inferring microstructural features and the physiological state of tissues from diffusion-weighted images. NMR in Biomedicine, vol 8, 333-344 (1995).

[7]. Basser, P.J., Jones DK. Diffusion-tensor MRI: theory, experimental design and data analysis-a technical review. NMR Biomed 2002; 15:456 – 67

[8]. Chabert S, Mecca CC, Le Bihan DJ. Relevance of the information about the diffusion distribution in invo given by kurtosis in q-space imaging. In: Proc 12th Annual Meeting ISMRM, Kyoto; 2004. p 1238.

[9]. Jensen, J. H., Helpern J. A.,Ramani, A., et al., Diffusional kurtosis imaging: the quantification of non-Gaussian water diffusion by means of magnetic resonance imaging. Magn Reson Med 2005; 53:1432– 40

[10]. Raab, P., Hattingen, E., Franz, K., Zanella, F.E., Lanfermann, H., Cerebral gliomas: diffusional kurtosis imaging analysis of microstructural differences. Radiology 2010; 254:876–881.

[11]. Wu, E.X., Cheung, M.M., MR diffusion kurtosis imaging for neural tissue characterization. NMR Biomed 2010; 23:836–848.

[12]. Fieremans, E., Jensen, J.H., Helpern, J.A., White matter characterization with diffusional kurtosis imaging. NeuroImage 2011; 58:177–188.

[13]. Koh, D.M., Collins, D.J., Diffusion-weighted MRI in the body: applications and challenges in oncology. AJR Am J Roentgenol 2007; 188:1622–1635.

[14]. Rosenkrantz, A. B., Sigmund, E. E., Johnson, G., et al. Prostate cancer: feasibility and preliminary experience of a diffusional kurtosis model for detection and assessment of aggressiveness of peripheral zone cancer. Radiology 2012; 264:126–135.

[15]. Jansen, J.F., Stambuk, H.E., Koutcher, J.A., Shukla-Dave, A., Non-Gaussian analysis of diffu-

sion-weighted MR imaging in head and neck squamous cell carcinoma: a feasibility study. AJNR Am J Neuroradiol 2010; 31:741–748.
[16]. Iima, M., Yano, K., Kataoka, M., et al. Quantitative non-Gaussian diffusion and intravoxel incoherent motion magnetic resonance imaging: differentiation of malignant and benign breast lesions. Invest Radiol 2015; 50:205–211.
[17]. Anderson, S.W., Barry, B., Soto, J., Ozonoff, A., O'Brien, M., Jara, H., Characterizing non-Gaussian, high b-value diffusion in liver fibrosis: stretched exponential and diffusional kurtosis modeling. J Magn Reson Imaging JMRI 2014; 39:827–834.
[18]. Jerome, N.P., Miyazaki, K., Collins, D.J. et al. Eur Radiol (2016). doi:10.1007/s00330-016-4318-2
[19]. Katahira K, Takahara T, Kwee TC, et al. Ultra-high-b-value diffusion- weighted MR imaging for the detection of prostate cancer: evaluation in 201 cases with histopathological correlation. Eur Radiol 2011;21:188–196.
[20]. Rosenkrantz A.B., Kong X, Niver BE, et al. Prostate cancer: comparison of tumor visibility on trace diffusion-weighted images and the apparent diffusion coefficient map. AJR Am J Roentgenol 2011; 196:123–129.
[21]. Rosenkrantz AB, Prabhu V, Sigmund EE, Babb JS, Deng FM, Taneja SS. Utility of diffusional kurtosis imaging as a marker of adverse pathologic outcomes among prostate cancer active surveillance candidates undergoing radical prostatectomy. AJR Am J Roentgenol 2013; 201:840–846.
[22]. Kitajima K, Kaji Y, Kuroda K, Sugimura K. High b-value diffusion- weighted imaging in normal and malignant peripheral zone tissue of the prostate: effect of signal-to-noise ratio. Magn Reson Med Sci 2008; 7:93–99.
[23]. Tamura C, Shinmoto H, Soga S, et al. Diffusion kurtosis imaging study of prostate cancer: preliminary findings. J Magn Reson Imaging JMRI 2014; 40:723–729.
[24]. Quentin M, Blondin D, Klasen J, et al. Comparison of different mathematical models of diffusion-weighted prostate MR imaging. Magn Reson Imaging 2012;30:1468–1474.
[25]. Quentin M, Pentang G, Schimmoller L, et al. Feasibility of diffusional kurtosis tensor imaging in prostate MRI for the assessment of prostate cancer: preliminary results. Magn Reson Imaging 2014; 32: 880–885.
[26]. Bourne RM, Panagiotaki E, Bongers A, Sved P, Watson G, Alexander DC. Information theoretic ranking of four models of diffusion attenuation in fresh and fixed prostate tissue ex vivo. Magn Reson Med 2014; 72:1418–1426.
[27]. Bourne, R.; Panagiotaki, E. Limitations and Prospects for Diffusion-Weighted MRI of the Prostate. Diagnostics 2016, 6, 21.
[28]. Toivonen J, Merisaari H, Pesola M, et al. Mathematical models for diffusion-weighted imaging of prostate cancer using b values up to 2000 s/mm: Correlation with Gleason score and repeatability of region of interest analysis. Magn Reson Med 2014
[29]. Panagiotaki E, Chan RW, Dikaios N, et al. Microstructural characterization of normal and malignant human prostate tissue with vascular, extracellular, and restricted diffusion for cytometry in tumours magnetic resonance imaging. Invest Radiol 2015;50:218–227.
[30]. Maas MC, Futterer JJ, Scheenen TW. Quantitative evaluation of computed high B value diffusion-weighted magnetic resonance imag- ing of the prostate. Invest Radiol 2013;48:779–786.
[31]. Ueno Y, Takahashi S, Kitajima K, et al. Computed diffusion-weighted imaging using 3-T magnetic resonance imaging for prostate cancer diagnosis. Eur Radiol 2013;23:3509–3516.
[32]. Yoshiko Ueno, Tsutomu Tamada, Vipul Bist, Caroline Reinhold, Hideaki Miyake, Utaru Tanaka, Kazuhiro Kitajima, Kazuro Sugimura and Satoru Takahashi, Multiparametric magnetic resonance imaging: Current role in prostate cancer management, International Journal of Urology (2016) 23, 550—557, doi: 10.1111/iju.13119, Review Article
[33]. S. Lucarini, L. Mazzoni, S. Chiti, S. Busoni, C. Gori, I. Menchi, Analysis of the dependence

on b-values of DWI signal model outcomes in peripheral healthy and cancerous prostate tissues, Congress ECR 2013, Poster No. B-0086, http://dx.doi.org/10.1594/ecr2013/B-0086
[34]. Mazzoni LN, Lucarini S, Chiti S, Busoni S, Gori C, Menchi I. Diffusion- weighted signal models in healthy and cancerous peripheral prostate tissues: comparison of outcomes obtained at different b-values. J Magn Reson Imaging JMRI 2014;39:512–518.
[35]. Suo S, Chen X, Wu L, et al. Non-Gaussian water diffusion kurtosis imaging of prostate cancer. Magn Reson Imaging 2014;32:421–427.
[36]. Jambor I, Merisaari H, Taimen P, et al. Evaluation of different mathematical models for diffusion-weighted imaging of normal prostate and prostate cancer using high b-values: a repeatability study. Magn Reson Med 2015;73:1988–1998.
[37]. Roethke MC, Kuder TA, Kuru TH, et al. Evaluation of diffusion kurtosis imaging versus standard diffusion imaging for detection and grading of peripheral zone prostate cancer. Invest Radiol 2015.
[38]. Merisaari H, Jambor I. Optimization of b-value distribution for four mathematical models of prostate cancer diffusion-weighted imaging using b values up to 2000 s/mm (2): Simulation and repeatability study. Magn Reson Med 2015;73:1954–1969.
[39]. R. Turner, M. K. Stehling, F. Schmitt. Echo-Planar Imaging: theory, technique and application. Springer (1998).
[40]. E. Stejskal, J. E. Tanner, Spin diffusion measurements: spin echoes in the presence of a time- dependent field gradient. J. Chem. Phys. 42, 288-292 (1954).
[41]. H.C.Torrey. Bloch equations with diffusion terms. Physical Review 104: 563-565 (1956).
[42]. Ciccarone, A., Mortilla, M.; Di Feo, D.; Lelli, L.; Leopardi, F.; Defilippi, C., Non-Gaussian Analysis of Diffusion-Weighted MR Imaging in pediatric brain: initial clinical results, European Society of Paediatric Radiology, 51st Annual Meeting, June 2-6 2014, Amsterdam
[43]. Mulkern R.V., Gudbjartsson H, Westin CF, et al. Multi-component apparent diffusion coefficients in human brain. NMR Biomed 1999;12:51– 62
[44]. Bennett KM, Schmainda KM, Bennett RT, et al. Characterization of continuously distributed cortical water diffusion rates with a stretched-exponential model. Magn Reson Med 2003; 50:727–34
[45]. Lu H, Jensen JH, Ramani A, et al. Three-dimensional characterization of non-gaussian water diffusion in humans using diffusion kurtosis imaging. NMR Biomed 2006;19:236 – 47
[46]. D.Le Bihan. Molecular Diffusion Nuclear Magnetic Resonance Imaging. Magnetic Resonance Quarterly: vol 7 No. 1: 1-30 (1991).
[47]. D.Le Bihan. Diffusion and perfusion magnetic resonance imaging. Applications to functional MRI. Raven Press – New York 1995.
[48]. Le Bihan D. The 'wet mind': water and functional neuroimaging. Phys Med Biol 2007;52:R57–90.
[49]. Rosenkrantz AB, Hindman N, Lim RP, et al. Diffusion-weighted imaging of the prostate: comparison of b1000 and b2000 image sets for index lesion detection. J Magn Reson Imaging JMRI 2013; 38:694–700.
[50]. Le Bihan D. Apparent diffusion coefficient and beyond: what diffusion MR imaging can tell us about tissue structure. Radiology 2013;268:318–322.
[51]. Grinberg F, Farrher E, Ciobanu L, Geffroy F, Le Bihan D, Shah NJ. Non-Gaussian diffusion imaging for enhanced contrast of brain tissue affected by ischemic stroke. PLoS One 2014;9:e89225.
[52]. Padhani AR, Makris A, Gall P, Collins DJ, Tunariu N, de Bono JS. Therapy monitoring of skeletal metastases with whole-body diffusion MRI. J Magn Reson Imaging JMRI 2014;39:1049–1078.
[53]. Nonomura Y, Yasumoto M, Yoshimura R, et al. Relationship between bone marrow cellularity and apparent diffusion coefficient. J Magn Reson Imaging JMRI 2001;13:757–760.
[54]. Le Bihan D. The 'wet mind': water and functional neuroimaging. Phys Med Biol

2007;52:R57–90.
[55]. Jensen JH, Helpern JA. MRI quantification of non-Gaussian water diffusion by kurtosis analysis. NMR Biomed 2010;23:698–710.
[56]. White NS, Dale AM. Distinct effects of nuclear volume fraction and cell diameter on high b-value diffusion MRI contrast in tumors. Magn Reson Med 2014;72:1435–1443.
[57]. Lawrence E, Goldman D, Gallagher F, et al. Evaluating the Relationship between Gleason Score, Tumor Tissue Composition, and Diffusion Kurtosis Imaging in Intermediate/High-risk Prostate Cancer Whole-mount Specimens. Radiological Society of North America 2014 Scientific Assembly and Annual Meeting, Chicago IL. http://archive. rsna.org/2014/14003112.html. Accessed April 26, 2015.
[58]. Panagiotaki E, Chan RW, Dikaios N, et al. Microstructural characterization of normal and malignant human prostate tissue with vascular, extracellular, and restricted diffusion for cytometry in tumours magnetic resonance imaging. Invest Radiol 2015;50:218–227.
[59]. Rosenkrantz AB, Sigmund EE, Winnick A, et al. Assessment of hepatocellular carcinoma using apparent diffusion coefficient and diffusion kurtosis indices: preliminary experience in fresh liver explants. Magn Reson Imaging 2012;30:1534–1540.
[60]. Goshima S, Kanematsu M, Noda Y, Kondo H, Watanabe H, Bae KT. Diffusion kurtosis imaging to assess response to treatment in hypervascular hepatocellular carcinoma. AJR Am J Roentgenol 2015; 204:W543–549.
[61]. Esposito, M. et al., PD-0145: Diffusional kurtosis as a biomarker of prostate cancer response to radiation therapy, Radiotherapy and Oncology, Volume 115 , S69 - S70
[62]. M. Esposito, P. Alpi, R. Barca, R. Carpi, S. Fondelli, A. Ghirelli, B. Grilli, Leonulli, L. Guerrini, S. Mazzocchi, D. Nizzi Grifi, M. Olmastroni, L. Paoletti, S. Pini, F. Rossi, S. Russo, G. Zatelli, P. Bastiani, Diffusional kurtosis as a biomarker of prostate cancer response to radiation therapy, ESTRO 2015, 3rd ESTRO Forum 24-28 April 2015, Barcelona, Spain
[63]. Giacomo Belli, Simone Busoni, Antonio Ciccarone, Angela Coniglio, Marco Esposito, Marco Giannelli, Lorenzo N. Mazzoni, Luca Nocetti, Roberto Sghedoni, Roberto Tarducci, Giovanna Zatelli, Rosa A. Anoja, Gina Belmonte, Nicola Bertolino, Margherita Betti, Cristiano Biagini, Alberto Ciarmatori, Fabiola Cretti, Emma Fabbri, Luca Fedeli, Silvano Filice, Christian P.L. Fulcheri, Chiara Gasperi, Paola A. Mangili, Silvia Mazzocchi, Gabriele Meliadò, Sabrina Morzenti, Linhsia Noferini, Nadia Oberhofer, Laura Orsingher, Nicoletta Paruccini, Goffredo Princigalli, Mariagrazia Quattrocchi, Adele Rinaldi, Danilo Scelfo, Gloria Vilches Freixas, Leonardo Tenori, Ileana Zucca, Claudio Luchinat, Cesare Gori, Gianni Gobbi. 2016. Quality assurance multicenter comparison of different MR scanners for quantitative diffusion-weighted imaging. Journal of Magnetic Resonance Imaging 43:10.1002/jmri.v43.1, 213-219.
[64]. Galanti, M., Fanelli, D., Traytak, S. D., and Piazza, F., Theory of diffusion-influenced reactions in complex geometries. Physical Chemistry Chemical Physics. DOI: 10.1039/C6CP01147K, Phys. Chem. Chem. Phys., 2016, 18, 15950-15954
[65]. Dmitry S. Novikov, Els Fieremans, Jens H. Jensen & Joseph A. Helpern, Random walks with barriers, , Nature Physics 7, 508–514 (2011) doi:10.1038/nphys1936
[66]. Dmitry S. Novikov, Jens H. Jensenb, Joseph A. Helpernb, and Els Fieremans, Revealing mesoscopic structural universality with diffusion, doi: 10.1073/pnas.1316944111, PNAS April 8, 2014 vol. 111 no. 14 5088-5093
[67]. Novikov, D. S. and Kiselev, V. G. (2010), Effective medium theory of a diffusion-weighted signal. NMR Biomed., 23: 682–697. doi: 10.1002/nbm.1584
[68]. Barucci, A., Ciccarone, A. Esposito, M., and G. Zatelli, Magnetic Resonance Spectroscopy Data Analysis for Clinical Applications, Thesis for the degree of Medical Physicist in the "Scuola di specializzazione in Fisica Medica", Scuola di Scienze della Salute Umana, Università degli studi di Firenze, P.zza S.Marco, 4 - 50121 Firenze, 2015.

[69]. "Magnetic Resonance Spectroscopy - Data Analysis for Clinical Applications", IFAC Book Series, ISBN 978-88-906859-9-6, di A. Barucci, R. Carpi, A. Ciccarone, M. Esposito, M. Olmastroni, G. Zatelli.